

The following scientific article was officially published in the journal *Computerized Medical Imaging and Graphics*, published by Elsevier. This article's citation is as follows:

Assi, Kondo Claude, Sebastien Grenier, Stefan Parent, Hubert Labelle, and Farida Cheriet. "A physically based trunk soft tissue modeling for scoliosis surgery planning systems." *Computerized Medical Imaging and Graphics*, Vol. 40, (2015): pp. 217-228.

doi: [10.1016/j.compmedimag.2014.11.002](https://doi.org/10.1016/j.compmedimag.2014.11.002)

The manuscript, as submitted in 2013 by the first author (preprint), is reproduced here, as it appears in the first author's Ph.D. thesis, entitled *Modélisation physique des tissus mous du tronc scoliotique pour la simulation de l'apparence post-chirurgicale*. The thesis citation is as follows:

Assi, Kondo Claude. "Modélisation physique des tissus mous du tronc scoliotique pour la simulation de l'apparence post-chirurgicale." PhD diss., École Polytechnique de Montréal, 2014.



Kondo Claude Assi, 2013

© 2013 Kondo Claude Assi. This work is licensed under the Creative Commons Attribution-NonCommercial-NoDerivatives 4.0 International License. To view a copy of this license, visit:

<http://creativecommons.org/licenses/by-nc-nd/4.0/>

CHAPITRE 4

ARTICLE 1: A PHYSICALLY BASED TRUNK SOFT TISSUE MODELING FOR SCOLIOSIS SURGERY PLANNING SYSTEMS

K. C. Assi^{1,2}, S. Grenier^{1,2}, S. Parent², H. Labelle², and F. Chretien^{1,2}

(1) *École Polytechnique de Montréal, P.O. Box 6097, Succursale Centre-ville, Montréal, Québec, Canada H3C 3A7*

(2) *Sainte-Justine Hospital Research Center, 3175 Côte-Sainte-Catherine, Montréal, Québec, Canada H3T 1C5*

4.1 Abstract

One of the major concerns of scoliotic patients undergoing spinal correction surgery is the trunk's external appearance after the surgery. This paper presents a novel incremental approach for simulating postoperative trunk shape in scoliosis surgery. Preoperative and postoperative trunk shapes data were obtained using three-dimensional medical imaging techniques for seven patients with adolescent idiopathic scoliosis. Results of qualitative and quantitative evaluations, based on the comparison of the simulated and actual postoperative trunk surfaces, showed an adequate accuracy of the method. Our approach provides a candidate simulation tool to be used in a clinical environment for the surgery planning process.

4.2 Introduction

Adolescent idiopathic scoliosis (AIS) is a complex three-dimensional deformation of the trunk. In severe cases, a spine surgery treatment is required. Most of the surgical procedures use specialized instrumentation attached to the spine to correct the deformities (Fig. 4.1). One

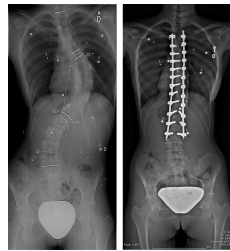


Figure 4.1 Surgical instrumentation of a scoliotic spine for the correction of spinal deformities. A. Preoperative radiograph. B. Postoperative radiograph.

of the concerns of the patient (and, in fact, a major factor of satisfaction) is the trunk's appearance after the surgery. In addition to the surgeon's priorities in the surgery planning process, a tool for simulating the trunk's postoperative appearance is of importance to take into account the patient's concerns in the treatment planning.

Aubin *et al.* [4] have developed a spinal surgery simulation system in the context of the optimal planning of surgical procedures to correct scoliotic deformities. The overall goal of this biomechanical engineering research project is to develop a user-oriented simulator for virtual prototyping of spinal deformities surgeries: a fully operational, safe and reliable patient-specific tool that will permit advanced planning of surgery with predictable outcomes, and rationalized design of surgical instrumentation [3, 4]. It addresses the problems faced by orthopedic surgeons treating spinal deformities when making surgical planning decisions. The developed system is, however, only concerned with the configuration of the spine, and does not furnish any estimate of the effects of the surgical treatment on the external appearance of the trunk. A desirable complement to this spine simulator would be to develop a full trunk model that would allow the propagation of the surgical correction on the spine toward the external trunk surface through the soft tissue deformation.

Physics-based models of deformable objects have been studied since the early 80's and are common in animation where physical laws are applied to an object to simulate realistic movements. Deformable physics-based models are also used in biomedical applications, in particular for surgery simulation [30]. These applications require visual and physical realism, but the real biomechanical properties involved are not always well known. The two most popular approaches to physically modeling soft tissues are the Finite Element Method (FEM) and Mass-Spring Model (MSM). Commonly used in engineering to accurately analyze structures and continua, the conventional FEM still has a large memory cost and computation times that limit interactive applications. Variants of FEM-based methods have thus been introduced to solve these issues [36, 38, 37]. However most of them are applicable only to linear deformations valid for small displacements. Improvements have been made to include large deformations in real-time [39] but a small number of elements must be considered in order to attain interactivity due to the increased computational cost. Application examples are the simulation of plastic and maxillofacial surgeries [31, 40, 2] and breast reconstructive surgery [41]. The MSM approach is less physically accurate than continuum biomechanical models. Nonetheless, with different stiffness springs, Terzopoulos and Waters [33] animated a face composed of several layers of springs representing the epidermis, dermis, sub-cutaneous connective tissue, fascia and muscles. A generic model was adapted to real digitized faces by an optimization of the masses' positions using facial features [80]. Koch *et al.* [31] used a finite element surface connected to the skull by springs to simulate a facial

plastic surgery. The MSM approach has also been used to model hip joint replacement [81]. In general, mass-spring methods have many advantages: simple implementation, intuitiveness, efficiency, good first interactive impression and easy parallelization. On the other hand, classical MSM present some disadvantages: (i) since no volume behavior of the tetrahedra is incorporated into the model, flip-over of springs may possibly occur; (ii) there is no way to control the volume conservation during simulation.

In general, large deformations of soft tissue are dealt with by introducing nonlinearities in the formulation of the tissue properties. Nonlinear elasticity has been proven to yield better results as compared to linear elasticity in the case of large deformations [37, 39]. However, the complexity of the computation is increased with this solution. In this paper, we propose a novel incremental approach for simulating the trunk shape correction that takes into account the large deformations involved in the preoperative-to-postoperative changes, while maintaining the linear approximation. The main idea consists in reducing the nonlinear deformation process into a sequence of small deformations for which the linear elastic behavior holds, so that one can keep the initial linear formalism in the course of the simulation. The method is then applied to a set of real data of scoliotic patients ($n = 7$) who have undergone spine surgery and for whom preoperative and postoperative data are available.

4.3 Methodology

4.3.1 The scoliotic patients sample

Consenting AIS patients ($n = 7$) with thoracic (spinal) curve having undergone corrective spine surgery at Sainte-Justine University Hospital Center in Montréal, Canada were considered. The hospital’s Research Ethics Committee has approved the study protocol. The average patient age at the time of surgery was 13.9 ± 1.5 (mean \pm standard deviation) years old, and Cobb angles before surgery averaged 65.3° (standard deviation: 1.5°).

4.3.2 Data acquisition and construction of patient-specific trunk geometric model

A non-invasive active vision system and a calibrated biplanar X-ray imaging system are used respectively to acquire the trunk surface topography and to reconstruct the 3D geometry of the trunk’s bone structures (spine, rib cage and pelvis). The surface geometry of the trunk is acquired using a calibrated system composed of four 3D optical digitizers (Creaform Inc., Levis, Canada), each one comprising a CCD camera and a structured light projector, placed around the patient (Fig. 5.1). The acquisition process, identical for each scanner, consists in projecting and capturing four fringe patterns deformed by the trunk’s external shape. The system then computes, by triangulation, the depth of each surface point relative

to the reference plane of the digitizer. A fifth image, captured without fringes, defines the texture data mapped on the surface. The entire trunk geometry is obtained by registering and merging the partial surfaces obtained by each digitizer. This process takes 4-6 seconds with the patient standing still in the upright position, arms slightly abducted to prevent occluded areas in the field of view of the lateral scanners. The resulting surface mesh (containing 50k-

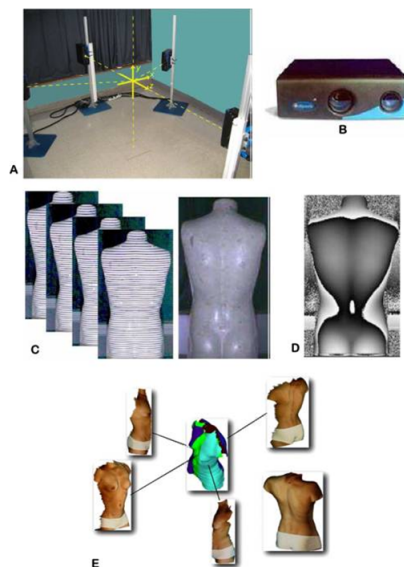


Figure 4.2 Trunk topography measurement and reconstruction. (A) Experimental set-up at Sainte-Justine Hospital of four Creaform optical digitizers. (B) Example of a Capturor II LF 3D optical digitizer, consisting of a CCD camera coupled with a structured light projector. (C) Set of four fringe images, each offset by $\frac{1}{4}$ phase, projected by a digitizer onto the back of a mannequin; the fifth image provided the surface texture. (D) Resulting phase image from the four fringe images; surface reconstruction uses the interferometry principle combined with active triangulation. (E) The process of registering and merging the partial surfaces from the different digitizers produces the complete trunk surface.

90k vertices, depending on the patient's height) was proven to have a reconstruction accuracy of 1.4mm over the whole torso (when applied to a mannequin). The 3D reconstruction of the bone structures (Fig. 5.2) has an accuracy evaluated at 2.1 ± 1.5 mm over a set of 3D positions of identified landmarks [20]. A detailed surface mesh of the patient's skeletal structures is then obtained by fitting a high-resolution atlas of 3D generic bone structures to the personalized data of the patient using dual kriging. The atlas was created using computed tomography scans of a dry cadaveric specimen and the accuracy of the resulting geometrical model was evaluated at 3.5 ± 4.1 mm [82]. The external trunk surface is then closed and registered with the bone structure data, and a tetrahedral mesh of the whole trunk is thereafter generated using Tetgen [83], a public domain tetrahedral mesh generator based on Shewchuk's Delaunay refinement algorithm [84].

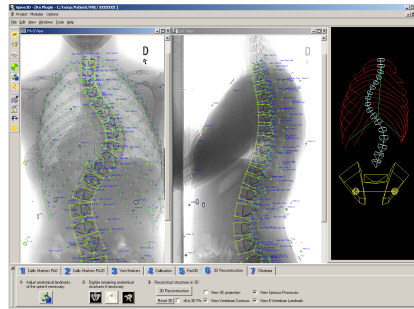


Figure 4.3 Graphical user interface of the system for 3D reconstruction of the bone structures. This view shows the identification of anatomical landmarks on the vertebrae and ribs in the coronal and sagittal radiographs (left and middle), and a simplified 3D reconstruction (right) [1].

4.3.3 Numerical simulation of postoperative trunk shapes

We introduce a novel incremental approach for simulating the trunk deformation. Fig. 4.4 represents a flow chart of our postoperative trunk appearance simulation system, where

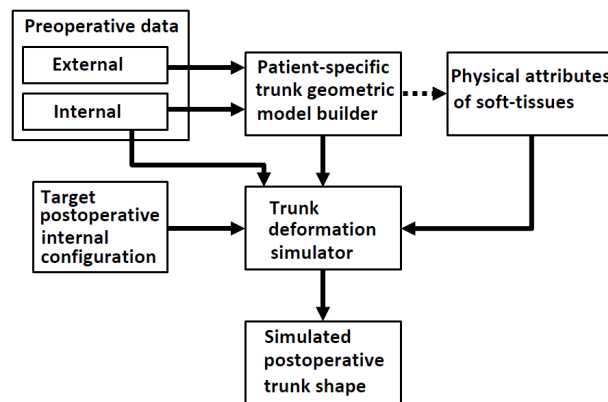


Figure 4.4 Flow chart of the postoperative trunk shape simulation.

only the key components of the simulation engine are indicated. The process starts with the preoperative data (the bone structures and the trunk surface). From these data, a patient-specific trunk geometry model is built. The resulting model along with the target postoperative internal configuration are then input into the trunk deformation simulator. The simulator outputs a new trunk shape which can then be further evaluated.

4.3.4 Modeling the trunk soft tissue deformation

The surgery of the scoliotic spine consists in attaching one or more metallic rods to the spine and performing certain maneuvers to correct its curvature. As a result of the change in the

spine configuration, one expects the whole trunk (and particularly the external surface) to change accordingly. We consider the human trunk as a deformable continuum occupying a bounded domain $\Omega \in \mathbb{R}^3$, with a continuous boundary Γ_Ω . A two-material body model (consisting in a bone structures region in Ω_b and a soft tissue region in $\Omega_s = \Omega \setminus \Omega_b$) is considered. In the following, spatial domains related to the preoperative trunk will be indicated by the superscript 0, while domains related to the postoperative trunk will be indicated by the superscript 1. One may view the trunk shape changes as follow: an arbitrary point in the trunk at $\mathbf{x}^0 \in \Omega^0$ is moved to a new position $\mathbf{x}^1 \in \Omega^1$, and the overall process induces a change from shape state Ω^0 to shape state Ω^1 .

Incremental approach to simulate the postoperative trunk external surface

From now on, we denote by $\mathcal{C}(\Omega)$ the space of smooth mappings from Ω to \mathbb{R}^3 , and $\mathcal{B}(\Omega)$ the subspace of $\mathcal{C}(\Omega)$ corresponding to small deformations on Ω . Let $\mathcal{E}(\omega, \Omega^0; \mathbf{f})$ denote the deformation energy required to deform Ω^0 into ω through a deformation $\mathbf{f} \in \mathcal{F}$, where \mathcal{F} denotes the space of (smooth) mappings such that

$$\mathcal{F} = \{\mathbf{f} \in \mathcal{C}(\Omega) | \mathbf{f}(\Omega_b^0) \approx \Omega_b^1\}.$$

Let us represent the deformation of a scoliotic trunk from the preoperative to the postoperative configurations by $\phi(\mathbf{x})$ for $\mathbf{x} = (x, y, z) \in \Omega^0$. By considering the principle of least action, the state of equilibrium of the postoperative trunk shape model is reached when the deformation energy is a minimum:

$$\begin{cases} \Omega^1 = \phi(\Omega^0), \\ \phi = \underset{\mathbf{f} \in \mathcal{F}}{\operatorname{argmin}} \left\{ \mathcal{E}(\omega, \Omega^0; \mathbf{f}) : \omega = \mathbf{f}(\Omega^0) \right\}, \end{cases} \quad (4.1)$$

for an energy functional $\mathcal{E}(\omega, \Omega^0; \mathbf{f})$ to be discussed later (Section 4.3.4). Eq. (4.1) may be rewritten as

$$\Omega^1 = \underset{\omega = \underset{\omega = \mathbf{f}(\Omega^0)}{\omega}}{\operatorname{argmin}} \left\{ \mathcal{E}(\omega, \Omega^0; \mathbf{f}) : \mathbf{f} \in \mathcal{F} \right\}. \quad (4.2)$$

While Eq. (4.1) is primarily concerned with the search for the deformation ϕ in the space of smooth mappings \mathcal{F} , Eq. (4.2) processes admissible shapes and selects the optimal one which is the deformed trunk shape at equilibrium. We define the space of mappings \mathcal{U} as

$$\mathcal{U} = \{\tilde{\mathbf{f}} \in \mathcal{C}(\Omega) | \tilde{\mathbf{f}}_{|\Omega_b} = \operatorname{Id}\},$$

where Id is the identity map. Let $\omega = \omega_s \cup \omega_b$ be a trunk shape variable. Let us define the mapping $\tilde{\varphi}$ (relaxation), $\tilde{\varphi}(\mathbf{x})$ for $\mathbf{x} \in \omega$, as follows:

$$\begin{aligned} \tilde{\varphi} &\in \mathcal{U}, \\ \tilde{\varphi}(\omega) &= \tilde{\omega}_s \cup \omega_b, \\ \tilde{\omega}_s &= \underset{\substack{\omega_s^+ \\ \omega_s^+ = \omega^+ \setminus \omega_b}}{\text{argmin}} \left\{ \mathcal{E}(\omega^+, \Omega^0; \tilde{\mathbf{f}}) : \right. \\ &\quad \left. \omega^+ = \tilde{\varphi}(\omega), \tilde{\mathbf{f}} \in \mathcal{U} \right\}, \end{aligned} \tag{4.3}$$

where $\mathcal{E}(\omega, \Omega^0; \mathbf{f})$ is the deformation energy model.

We now introduce a novel incremental approach for the simulation of postoperative trunk shape. Let $(t_k)_{k=0,1,2,\dots,N}$ be a sequence of real numbers such that $t_k \in [0, 1]$, $t_{k+1} > t_k$ for $k \in \{0, 1, 2, \dots, N-1\}$, $t_0 = 0$ and $t_N = 1$. Let $L^0 = \{\mathbf{I}_i^0 \in \Omega_b^0, i = 1, \dots, n\}$ and $L^1 = \{\mathbf{I}_i^1 \in \Omega_b^1, i = 1, \dots, n\}$ be, respectively, a collection of landmarks on the preoperative bone structures and the collection of corresponding anatomical landmarks on the target postoperative bone configuration. Let \mathcal{S} denote the space of smooth transformations, defined as

$$\mathcal{S} = \{ \mathbf{f} \in \mathcal{C}(\Omega) \mid \mathbf{f}(\mathbf{I}_i^0) \approx \mathbf{I}_i^1, i = 1, \dots, n \}.$$

We have $\mathcal{S} \subset \mathcal{F}$. Let \mathcal{G}_0 denote the collection of sequences of transformations $\Phi = (\phi_{t_k})_{k=0,\dots,m}$, with small increments (See definition in 4.6, Definition 1), such that

$$\begin{aligned} \mathcal{G}_0 &= \left\{ (\phi_{t_k})_{k=0,\dots,m} \in \mathcal{G}, \quad m \in \mathbb{N} \quad \mid \quad \phi_{t_0} = \text{Id}_{\mathbb{R}^3}, \right. \\ &\quad \left. \phi_{t_m} \circ \phi_{t_{m-1}} \circ \dots \circ \phi_{t_1} \circ \phi_{t_0} \in \mathcal{S} \right\}. \end{aligned} \tag{4.4}$$

Our incremental approach defines a sequence of trunk shapes $(\Omega^{t_k})_{k=0,1,\dots,m}$, $m \in \mathbb{N}$, moving from the undeformed state Ω^0 to the deformed state Ω^1 based on a sequence of mappings $\Phi \in \mathcal{G}_0$. Let $\Omega_b^{t_k}$ and $\Omega_s^{t_k}$ be, respectively, the bone and soft tissue configurations of the trunk shape Ω^{t_k} ($\Omega^{t_k} = \Omega_s^{t_k} \cup \Omega_b^{t_k}$) at increment step k , within the sequence starting at Ω^0 under successive deformations. Our method computes Ω^1 as the final shape of the sequence

$(\Omega^{t_k})_{k=0,1,2,\dots,N}$ as follows:

$$\begin{aligned}\Omega^0 &= \Omega_s^0 \cup \Omega_b^0, \\ \Omega^{t_k} &= \Omega_s^{t_k} \cup \Omega_b^{t_k}, \quad k = 0, 1, \dots, N, \\ \Omega^{t_{k+1}} &= \tilde{\varphi} \circ \phi_{t_{k+1}}(\Omega^{t_k}), \quad (\phi_\tau)_{0 \leq \tau \leq 1} \in \mathcal{G}_0.\end{aligned}\tag{4.5}$$

In Algorithm (4.5), the first equation refers to the initial state of the trunk, the second one refers to the indexed trunk shape state at increment step t_k , and the third one states the transition rule from step k to step $k+1$. Our first analytical result deals with the properties of independence of the final equilibrium state from the chosen sequence $\Phi \in \mathcal{G}_0$. These properties are established by Theorem 1 and Theorem 2 (See 4.6). Our second analytical result establishes that Algorithm (4.5) gives the solution to the problem stated in Eq. 4.2 (See 4.6, Theorem 3). In this paper, we consider a family of thin plate spline mappings, $(\phi_{t_k})_{k=0,1,\dots,N} \in \mathcal{G}_0$, associated with the matching of the bone structure landmarks.

The incremental approach proposed in this section is usable for any appropriate deformation energy functional of the trunk. In the next section, we address a specific energy model to be used in the present work.

Deformation energy model

Let us assume that we have a conformal tetrahedral mesh describing the geometry of the anatomical structures of the trunk. We denote the mesh at its rest position as \mathcal{M}^0 and the initial position of each vertex as \mathbf{P}_i^0 . We denote the vertex position of a deformed mesh \mathcal{M}^1 as \mathbf{P}_i . Let us represent the deformation by a displacement vector field $\mathbf{U}(\mathbf{x})$ for $\mathbf{x} = (x, y, z) \in \mathcal{M}^0$, and we write $\mathbf{f} = \text{Id} + \mathbf{U}$, where Id is the identity transformation. Given a deformed model \mathcal{M}^1 , let us define the displacement vector for each point of the domain by linearly interpolating the displacement $\mathbf{U}_i \equiv \mathbf{P}_i - \mathbf{P}_i^0$ of the vertices inside each tetrahedron. If T_i represents the tetrahedron defined by the four vertices \mathbf{P}_j^0 , $j = 1, \dots, 4$, in their rest position, then the displacement vector at a given point $\mathbf{x} = (x, y, z)$ is defined as:

$$\mathbf{U}_{T_i}(\mathbf{x}) = \sum_{j=1}^4 a_j^{T_i}(\mathbf{x}) \mathbf{U}_j,$$

where $a_j^{T_i}(\mathbf{x})$ are the barycentric coordinates of the point \mathbf{x} inside T_i . The deformation energy $W_{T_i}(\mathbf{U})$ of a tetrahedron T_i can be expressed as an expansion over its features (characterized

by $\{\mathbf{P}_{T_i(j)}, j = 0, \dots, 3\}$, its vertices coordinates) as:

$$W_{T_i} = \sum_j W_j^{T_i} + \sum_{j,k} W_{jk}^{T_i} + \sum_{j,k,l} W_{jkl}^{T_i} + W_{jklm}^{T_i},$$

where the terms $W_j^{T_i}$, $W_{jk}^{T_i}$, $W_{jkl}^{T_i}$, and $W_{jklm}^{T_i}$, are the energy contributions from the nodes, edges, faces (triangles) and volume, respectively. The total deformation energy \mathcal{E} required to deform \mathcal{M}^0 into \mathcal{M}^1 is the sum of the energies associated with each tetrahedron:

$$\mathcal{E}(\mathcal{M}, \mathcal{M}^0; \mathbf{f}) = \sum_{T_i \in \mathcal{M}} W_{T_i}.$$

Incompressible Tetrahedral Mass System Model The incompressible tetrahedral mass system model (ITMSM), in its original form, was introduced by Teschner *et al.* [85]. The model has some similarities with the FEM and MSM approaches, in that it is based on a tetrahedral discretization of the deformed domain. We adapt the original deformable model [85] to take into account the contribution of gravity. The energy \mathcal{W}_T of a tetrahedron T in the soft tissue mesh is given by:

$$\mathcal{W}_T = \alpha \tilde{\mathcal{E}}_G + \tilde{\mathcal{E}}_D + \epsilon \tilde{\mathcal{E}}_A + \theta \tilde{\mathcal{E}}_V \quad (4.6)$$

with $\alpha = \frac{2gM_0H_0}{k_D}$, $\epsilon = \frac{k_A}{k_D}$ and $\theta = \frac{k_V}{k_D}$. The energy terms $\tilde{\mathcal{E}}_G$, $\tilde{\mathcal{E}}_D$, $\tilde{\mathcal{E}}_A$ and $\tilde{\mathcal{E}}_V$ are given by:

$$\tilde{\mathcal{E}}_G = \sum_{i \in T} \tilde{W}_i \quad (4.7)$$

$$\tilde{\mathcal{E}}_D = \sum_{i \neq j \in T} \frac{1}{|\mathcal{K}_{ij}|} \tilde{W}_{ij} \quad (4.8)$$

$$\tilde{\mathcal{E}}_A = \sum_{i \neq j \neq k \in T} \frac{1}{|\mathcal{K}_{ijk}|} \tilde{W}_{ijk} \quad (4.9)$$

$$\tilde{\mathcal{E}}_V = \tilde{W}_{ijkl} \quad (4.10)$$

where \mathcal{K}_{ij} and \mathcal{K}_{ijk} are the collections of tetrahedra in the soft tissue mesh containing edge ij and face ijk , respectively ($|\mathcal{K}_{ij}|$ and $|\mathcal{K}_{ijk}|$ represent the cardinality of these collections).

\widetilde{W}_i , \widetilde{W}_{ij} , \widetilde{W}_{ijk} and \widetilde{W}_{ijkl} are given by:

$$\widetilde{W}_i = - \left(\frac{m_i}{M_0} \right) \left(\frac{\mathbf{P}_i \cdot \mathbf{z}}{H_0} \right) \quad (4.11)$$

$$\widetilde{W}_{ij} = \left(\frac{\|\mathbf{P}_{ji}\| - D_0}{D_0} \right)^2 \quad (4.12)$$

$$\widetilde{W}_{ijk} = \left(\frac{\frac{1}{2} \|\mathbf{P}_{ji} \times \mathbf{P}_{ki}\| - A_0}{A_0} \right)^2 \quad (4.13)$$

$$\widetilde{W}_{ijkl} = \left(\frac{\frac{1}{6} \mathbf{P}_{ji} \cdot (\mathbf{P}_{ki} \times \mathbf{P}_{li}) - V_0}{V_0} \right)^2 \quad (4.14)$$

where $\mathbf{P}_{ji} = \mathbf{P}_j - \mathbf{P}_i$, \mathbf{z} is the vertical upward oriented unit vector and m_i is the partial mass associated to mass point \mathbf{x}_i , defined as:

$$m_i = \frac{1}{4} \rho_T V_T, \quad (4.15)$$

with ρ_T representing the local density of the tissue and V_T the volume of tetrahedron T . The initial distance or rest length of the edge is denoted by D_0 , A_0 is the initial area of the triangle and V_0 is the initial volume of the tetrahedron. The mean tetrahedral mass and the trunk height are respectively M_0 and H_0 , while k_D is the stiffness associated to tetrahedra edges (considered uniform throughout the soft tissue). The coefficients θ and ϵ introduced in Eq. (4.6) are the weights of the different potential energy contributions: θ is the stiffness ratio between volume- and distance-preserving energies, while ϵ is the stiffness ratio between area- and distance-preserving energies. The coefficients α , ϵ and θ are empirically determined. See the properties of the energy model in 4.6 (Lemma 3 and Theorem 4). We coined the name ITMSM for our model due to the tetrahedron volume energy term appearing in the model, which acts as an incompressibility constraint.

4.3.5 Evaluation of the simulation

Evaluations are conducted using the preoperative and postoperative data of scoliotic patients (3D reconstructions of the bone structures and trunk surface geometry acquisitions). First, a 3D visualization allows for a qualitative comparison of the simulated and the real postoperative trunk shapes. Then, the simulation accuracy is evaluated based on the measurement of the back surface rotation (BSR) on the simulated trunk and on the actual postoperative trunk, at thoracic vertebral levels between $T4$ (4th thoracic vertebra) and $T12$ (12th thoracic vertebra). The BSR index is measured in a series of horizontal cross-sections of the external trunk surface. It is defined as the angle formed between the dual tangent to the posterior

side of a given cross-section and the axis passing through the patient's anterior superior iliac spines (ASIS), projected onto the axial plane. This trunk asymmetry index is widely considered to be clinically relevant in the study of the scoliotic trunk shape [86]. We exploit

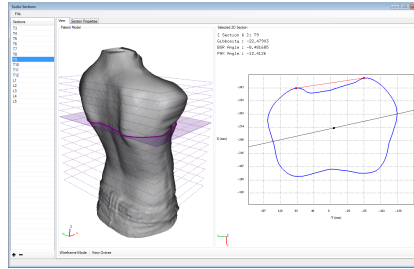


Figure 4.5 Graphical user interface of the software tool used to compute the BSR indices from cross-sections at various vertebral levels

the BSR index for our quantitative evaluation as follows. First, by exploiting a common set of radio-opaque markers purposely placed on the skin surface, an elastic registration of the trunk surface geometry with the internal bone structures is performed [87]. Trunk surface cross-sections are then extracted by computing the intersections of the surface topography (mesh) with a set of horizontal planes passing through the centroids of the vertebrae. Finally, the BSR index at each vertebral level is measured from the associated trunk horizontal cross section (Fig. 4.5).

4.4 Results

Simulation results for a patient are presented in Fig. 4.6, where a qualitative comparison of the preoperative trunk surface (Fig. 4.6-A), the simulated postoperative surface (Fig. 4.6-B) and the actual postoperative trunk shape (Fig. 4.6-C) is shown. A visual inspection of the

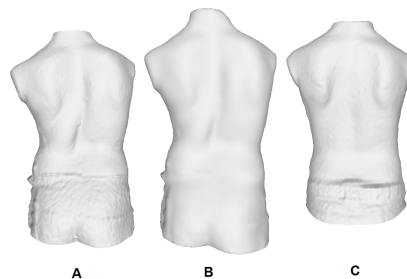


Figure 4.6 Example of simulation results. (A) Preoperative patient trunk, (B) simulated trunk shape, (C) real postoperative trunk.

results for all the patients in our test set shows a qualitative similarity between the simulated postoperative trunk shape and the real postoperative trunk shape. The overall appearance of the postoperative trunk is qualitatively well reproduced. The region of the back along the spine (back valley) is satisfactorily well reproduced. However, a rib hump is still observable on the simulated trunk surface when compared to the actual postoperative trunk, and the actual shape is less well reproduced in the lumbar region of the back. As well, some discrepancies are noticeable in the upper region of the back around the scapulae.

For the present study, the thoracic region was considered as the main region of interest of the scoliotic trunk, since the rib humps are located in that part of the body. The BSR indices measured at different vertebral levels on the simulated postoperative trunks are compared with those measured on the actual postoperative and preoperative trunks of six patients (Fig. 4.7). For these case studies, which are all characterized by a thoracic spinal curve, the simulated trunks are quantitatively close to the actual postoperative trunk surfaces. This is consistent with the results of the qualitative comparison. The mean absolute error of the BSR index measured on the simulated trunks ranges from $1.20^\circ (\pm 0.73^\circ)$ to $3.2^\circ (\pm 0.83^\circ)$ in the thoracic region.

The seventh case study is a patient characterized by a double major spinal curve. It is presented separately in Fig. 4.8 since it exhibits a relatively high discrepancy between the simulated and actual trunk shapes, compared to the other cases. The mean absolute error of the BSR index on the simulated trunks, for double major and thoraco-lumbar curves patients, range from $3.1^\circ (\pm 1.45^\circ)$ to $5.23^\circ (\pm 1.44^\circ)$, in the thoracic region.

4.5 Discussion

In the present work, the BSR index has been considered as an evaluation metric for the postoperative trunk simulation outcomes. This choice is appropriate since the patient's first concern is for their trunk asymmetry and the BSR quantity has been proven to capture the information related to the rotation of the trunk and the rib hump [86, 87, 88].

A smallest detectable difference of 2.5° for the maximum BSR index was reported by Pazos et al.[88] and therefore it is considered here as a threshold value to judge the accuracy of the simulation with regard to trunk asymmetry. The method proposed in the present work produced simulated postoperative trunks that are not only qualitatively similar to their real counterparts but that also quantitatively fall within the acceptable error range for the BSR index in the thoracic region, as given by the threshold value.

One source of discrepancy in the simulated trunk shapes may be the effect of posture, i.e. differences in standing posture between the pre- and post-operative trunk acquisitions. Simi-

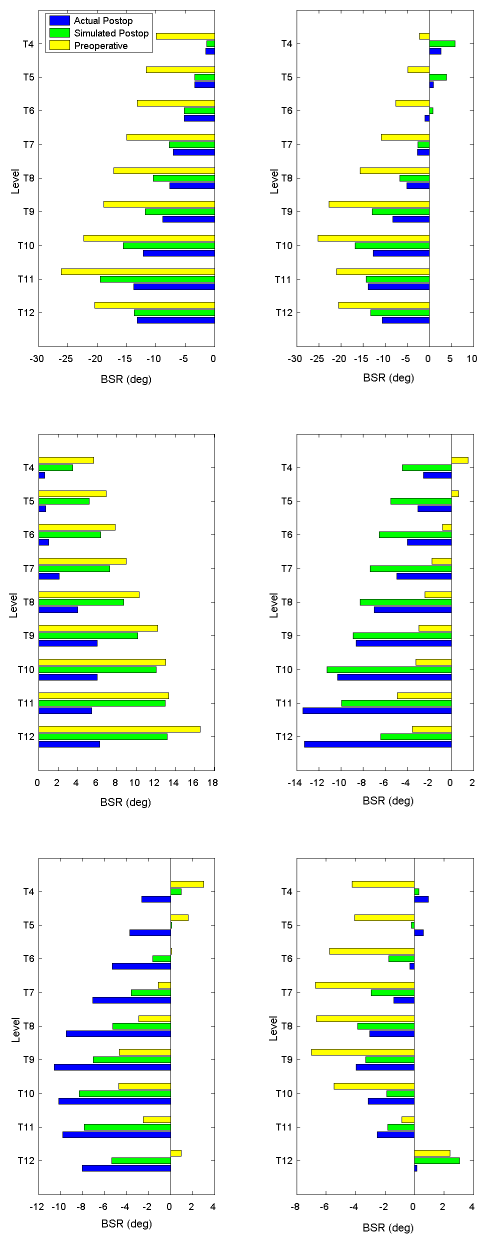


Figure 4.7 BSR indices (in degrees), measured at different vertebral levels from $T4$ to $T12$, for six patients. Blue: actual postoperative trunk, green: simulated trunk, yellow: preoperative trunk. Note that the horizontal scales are not the same on all the graphs.

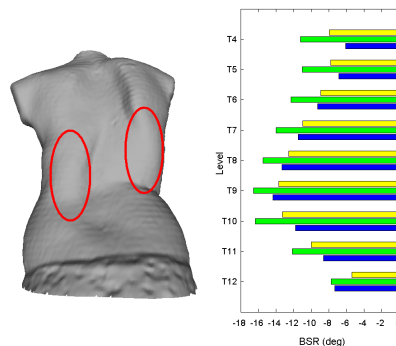


Figure 4.8 Left: Double major curve scoliotic patient (preoperative geometry). Right: BSR indices measured on the actual postoperative trunk, the simulated trunk and the preoperative trunk surface. Blue: actual postoperative trunk, green: simulated trunk, yellow: preoperative trunk.

larly, another factor is possible weight change (i.e loss or gain) between the preoperative and postoperative acquisitions. Of course, such factors would be difficult to remove totally. However, other sources of discrepancy may be attributed to certain limitations of our approach. Firstly, we considered uniform tissue materials properties throughout the trunk instead of more realistic nonuniform physical properties. Indeed, the soft tissues were approximated by a uniform volumetric mesh and no differentiation was made between actual soft tissue layers (i.e. skin, fat, muscles). This may have affected the accuracy of the simulation. Secondly, materials property coefficients were tuned manually since we have not yet implemented a rigorous method to provide them to the simulator. Finally, a monolithic/non-articulated organization of the bone structures was used, and this does not reflect the exact configuration of the spine.

In future work, some of the present limitations will be addressed. In particular, a personalized tetrahedral mesh can be obtained from MRI images of the trunk, from which the thickness of each tissue layer (skin, fat, muscle) can be extracted. This clinical data will be incorporated into the model and will allow us to simulate the propagation of the spinal correction to the external surface through a mesh composed of three personalized layers. Additionally, we believe that the accuracy of the simulation will be improved by using rigidity constants calibrated from real data of a representative cohort of scoliotic patients with different types of spinal curvature.

In addition, our team is currently developing a non invasive tool to assess the reducibility of the trunk deformity by using the acquisition of the external trunk surface in voluntary lateral bending position. This could lead to new constraints that will be incorporated into our model to simulate the propagation of the spinal correction through the tetrahedral mesh

composed of three personalized layers.

4.6 Conclusion

Spinal correction surgery treats deformities of the trunk bone structures. Since the external appearance of the trunk is one of the main concerns of the patient and one of the factors of his/her satisfaction, a surgery planning strategy that takes into account the outcome for the external 3D shape of the trunk would be a significant contribution.

In this paper, we presented an incremental approach to the soft tissue deformation problem for the simulation of the postoperative trunk shape of scoliotic patients. The evaluation of the method was based on the preoperative and postoperative clinical data of scoliotic patients who underwent spine correction surgery. Although the soft tissues of the human trunk were approximated by a uniform volumetric mesh, our method achieves promising results in the simulation of the postoperative trunk surface.

Conflict of interest statement

The authors declare that there are no conflicts of interest.

Acknowledgments

This research was funded by the Natural Sciences and Engineering Research Council of Canada. The equipment was financed by the Canadian Foundation for Innovation. Author 1 was supported, in part, by the Fondation Sainte-Justine and Fondation des Étoiles foundations of Sainte-Justine University Hospital Center. All the authors are grateful to Philippe Labelle, who performed the initial calibration of the data. We would also like to thank Philippe Debanné for his useful comments and for providing some of the data.

APPENDIX: Modeling the trunk soft tissue deformation

Our first analytical result deals with the properties of independence of the final equilibrium state from the chosen sequence of small incremental mappings. First, we introduce the following definition of a sequence of mappings of small increments.

Definition 1. *We say that a sequence of mappings $\Phi = (\phi_{t_k})_{k \in \{0, \dots, m\}}$ is of small increments if $\delta\Phi_{k,k-1} \in \mathcal{B}(\Omega)$ for all $k \in \{1, \dots, m\}$, where $\delta\Phi_{k,k-1} \equiv \phi_{t_k} \circ \phi_{t_{k-1}} - \phi_{t_{k-1}}$. We write: $\Phi \in \mathcal{G}$.*

For small deformations of the trunk, we then have:

Theorem 1. Let Ω^0 and Ω^1 be preoperative and postoperative trunks where Ω^1 resulted from a small deformation of Ω^0 and let $\mathcal{H} = \{\mathbf{h} \in \mathcal{C}(\Omega^0) | \mathbf{h}(\Omega_b^0) = \Omega_b^1\}$. Then $\tilde{\Omega}^* = \tilde{\varphi} \circ g(\Omega^0)$ is independent of g for $g \in \mathcal{H}$.

Proof. Let $g_1, g_2 \in \mathcal{B}(\Omega)$ be two arbitrary smooth and small deformations on Ω . Let $\omega_1^* = \tilde{\varphi} \circ g_1(\omega^0)$. Then, by definition, $\omega_1^* = \tilde{\omega}_s^* \cup g_1(\omega_b^0)$, with

$$\tilde{\omega}_s^* = \underset{\substack{\omega_s^+ \\ \omega_s^+ = \omega^+ \setminus g_1(\omega_b^0)}}{\operatorname{argmin}} \left\{ \mathcal{E}(\omega^+, \Omega^0; \tilde{\mathbf{f}}) : \right. \\ \left. \omega^+ = \tilde{\mathbf{f}}(\omega), \tilde{\mathbf{f}} \in \mathcal{U} \right\},$$

Let $\omega_2^* = \tilde{\varphi} \circ g_2(\omega^0)$. Then $\omega_2^* = \tilde{\omega}_s^{**} \cup g_2(\omega_b^0)$, with

$$\tilde{\omega}_s^{**} = \underset{\substack{\omega_s^+ \\ \omega_s^+ = \omega^+ \setminus g_2(\omega_b^0)}}{\operatorname{argmin}} \left\{ \mathcal{E}(\omega^+, \Omega^0; \tilde{\mathbf{f}}) : \right. \\ \left. \omega^+ = \tilde{\mathbf{f}}(\omega), \tilde{\mathbf{f}} \in \mathcal{U} \right\},$$

Since $g_1, g_2 \in \mathcal{B}(\Omega)$, we have $g_1(\omega_b^0) = g_2(\omega_b^0) = \omega_b^1$. Thus,

$$\tilde{\omega}_s^{**} = \underset{\substack{\omega_s^+ \\ \omega_s^+ = \omega^+ \setminus \omega_b^1}}{\operatorname{argmin}} \left\{ \mathcal{E}(\omega^+, \Omega^0; \tilde{\mathbf{f}}) : \omega^+ = \tilde{\mathbf{f}}(\omega), \tilde{\mathbf{f}} \in \mathcal{U} \right\} = \tilde{\omega}_s^*$$

and

$$\omega_1^* = \tilde{\omega}_s^* \cup \omega_b^1 = \tilde{\omega}_s^{**} \cup \omega_b^1 = \omega_2^*.$$

This establishes the conclusion of Theorem 1. \square

For large deformations of the trunk, we have:

Theorem 2. Let N_1 and N_2 be two positive integers, and let $\mathbf{G}^{(1)} = (g_{t_{k_1}}^{(1)})_{k_1=0, \dots, N_1}$, $\mathbf{G}^{(2)} = (g_{t_{k_2}}^{(2)})_{k_2=0, \dots, N_2}$, be two sequences of mappings, with $\mathbf{G}^1, \mathbf{G}^2 \in \mathcal{G}_0$. Let $g^{(1)} = (\tilde{\varphi} \circ g_{t_{N_1}}^{(1)}) \circ \dots \circ (\tilde{\varphi} \circ g_{t_0}^{(1)})$ and $g^{(2)} = (\tilde{\varphi} \circ g_{t_{N_2}}^{(2)}) \circ \dots \circ (\tilde{\varphi} \circ g_{t_0}^{(2)})$, where $\tilde{\varphi}$ is defined in section 4.3.4. Then $g^{(2)}(\omega^0) = g^{(1)}(\omega^0)$.

Proof. Let $\gamma^{(i)} = g_{t_{N_i}}^{(i)} \circ (\tilde{\varphi} \circ g_{t_{N_i-1}}^{(i)}) \circ \dots \circ (\tilde{\varphi} \circ g_{t_0}^{(i)})$, $i = 1, 2$. Then $g^{(i)} = \tilde{\varphi} \circ \gamma^{(i)}$, $i = 1, 2$. By the definition of \mathcal{G}_0 and $\tilde{\varphi}$, we have $\omega_b^{*(1)} = \gamma^{(1)}(\omega_b^0) = \gamma^{(2)}(\omega_b^0) = \omega_b^{*(2)}$, and $g^{(i)}(\omega^0) = \omega^{*(i)} =$

$\tilde{\omega}_s^{*(i)} \cup \omega_b^{*(i)} = \tilde{\omega}_s^{*(i)} \cup \gamma^{(i)}(\omega_b^0)$, with

$$\tilde{\omega}_s^{*(i)} = \underset{\substack{\omega_s^+ \\ \omega_s^+ = \omega^+ \setminus \omega_b^{*(i)}}}{\operatorname{argmin}} \left\{ \mathcal{E}(\omega^+, \Omega^0; \tilde{\mathbf{f}}) : \right. \\ \left. \omega^+ = \tilde{\mathbf{f}}(\gamma^{(i)}(\omega^0)), \tilde{\mathbf{f}} \in \mathcal{U} \right\}, i = 1, 2.$$

Thus, $\omega_s^{*(1)} = \omega_s^{*(2)}$. It follows that $g^{(1)}(\omega^0) = g^{(2)}(\omega^0)$. \square

Our second analytical result deals with the solution of the problem stated in Eq. 4.2. We have the following:

Theorem 3. *For any $\mathbf{F} = (f_{t_j})_{j=0,1,\dots,m} \in \mathcal{G}_0$, if $\tilde{\Omega}^*$ is the final deformed shape of the sequence $(\Omega^{t_j})_{j=0,1,\dots,m}$ produced by Algorithm (4.5), then $\tilde{\Omega}^*$ satisfies Eq. (4.2), that is,*

$$\mathcal{E}(\tilde{\Omega}^*) = \min_{\substack{\omega \\ \omega = \mathbf{f}(\Omega^0)}} \left\{ \mathcal{E}(\omega, \Omega^0; \mathbf{f}) : \mathbf{f} \in \mathcal{F} \right\}.$$

In order to prove Theorem 3, we need the following lemmas:

Lemma 1. *Let $\mathbf{F} = (f_{t_j})_{j=0,\dots,m} \in \mathcal{G}_0$ be a fixed sequence. Let $\hat{\phi}_m, \hat{\phi}_{m-1}, \dots, \hat{\phi}_0 \in \mathcal{U}$. Then $(\hat{\phi}_m \circ f_{t_m}) \circ \dots \circ (\hat{\phi}_0 \circ f_{t_0}) \in \mathcal{F}$.*

Proof. Let $h = (\hat{\phi}_m \circ f_{t_m}) \circ \dots \circ (\hat{\phi}_0 \circ f_{t_0})$. Then h is smooth since the composition of smooth functions is smooth. Furthermore, $h \in \mathcal{F}$ since $\hat{\phi}_j|_{\omega_b^0} = \operatorname{Id}$, and we have $h(\Omega_b^0) = (\hat{\phi}_m \circ f_{t_m}) \circ \dots \circ (\hat{\phi}_0 \circ f_{t_0})(\Omega_b^0) = f_{t_m} \circ \dots \circ f_{t_0}(\Omega_b^0) = \Omega_b^1$. \square

The next lemma states that any smooth function can be expressed as the composition of a sequence of small deformations.

Lemma 2. *Suppose $\mathbf{F} = (f_{t_j})_{j=0,\dots,m} \in \mathcal{G}_0$ is given. For any $f \in \mathcal{F}$, there exists $\hat{\phi}_m, \hat{\phi}_{m-1}, \dots, \hat{\phi}_0 \in \mathcal{U}$ such that $f = (\hat{\phi}_m \circ f_{t_m}) \circ \dots \circ (\hat{\phi}_0 \circ f_{t_0})$.*

Proof. Let us consider an arbitrary $\hat{\phi}_{m-1}, \dots, \hat{\phi}_0 \in \mathcal{U}$ (for example, one can consider $\hat{\phi}_{m-1} = \dots = \hat{\phi}_0 = \tilde{\phi}$ where $\tilde{\phi}$ is defined in section 4.3.4). Let us define $f_m = f_{t_m} \circ (\hat{\phi}_{m-1} \circ f_{t_{m-1}}) \circ \dots \circ (\hat{\phi}_0 \circ f_{t_0})$. Then $\bar{\phi}_m = f - f_m \in \mathcal{U}$ (small deformation and $\bar{\phi}_m|_{\Omega_b} = \operatorname{Id}$), and we have $f = \bar{\phi}_m \circ f_m$ which has the desired form. \square

Finally, let us prove that Ω^* produced by Algorithm (4.5) satisfies Eq. (4.2). Let us write $\phi^* = (\tilde{\varphi} \circ f_{t_m}) \circ \dots \circ (\tilde{\varphi} \circ f_{t_0})$. Then, from Algorithm (4.5), we have $\tilde{\Omega}^* = \phi^*(\Omega^0)$. By Lemma 2, for any $f \in \mathcal{F}$, there exists $\hat{\phi}_m, \hat{\phi}_{m-1}, \dots, \hat{\phi}_0 \in \mathcal{U}$ such that $f = (\hat{\phi}_m \circ f_{t_m}) \circ \dots \circ (\hat{\phi}_0 \circ f_{t_0})$. The mapping ϕ^* produces the sequence of shapes $(\tilde{\Omega}^{t_j})_{j=0,\dots,m}$ to which is associated the sequence

of energies $\mathcal{E}_0^*, \mathcal{E}_1^*, \dots, \mathcal{E}_m^*$. On the other hand, f (through its expansion) produces the sequence of shapes $(\bar{\Omega}^{t_j})_{j=0, \dots, m}$ to which is associated the sequence of energies $\bar{\mathcal{E}}_0^*, \bar{\mathcal{E}}_1^*, \dots, \bar{\mathcal{E}}_m^*$. From the definition of $\tilde{\varphi}$, we have $\mathcal{E}_j^* \leq \bar{\mathcal{E}}_j^*$, $j = 0, \dots, m$. Thus, it follows that

$$\mathcal{E}(\tilde{\Omega}^*) = \mathcal{E}(\tilde{\Omega}^{t_m}) \leq \mathcal{E}\{\omega : \omega = f(\Omega^0), f \in \mathcal{F}\}.$$

This establishes the conclusion of Theorem 3 \square .

The energy model presented in the paper has the following property:

Lemma 3. *The energy functional $\mathcal{E}(\Omega, \Omega^0; \mathbf{f})$, given by Eq. (4.6), is (strictly) convex.*

Proof. The energy \mathcal{E} is a superposition of convex functions. It follows that \mathcal{E} is convex. \square

It follows that the trunk shape obtained by solving the optimization problem has the following property, stated as a theorem:

Theorem 4. *The optimal shape from Eq. (4.2), associated with the energy functional from Eq. (4.6), is unique.*

Proof. Since the energy functional is convex, a local minimum is also a global minimum. The conclusion of Theorem 4 follows, since the global minimum of a convex functional is unique. \square

RÉFÉRENCES

- [1] S. Kadoury, F. Cheriet, C. Laporte, and H. Labelle. A versatile 3D reconstruction system of the spine and pelvis for clinical assessment of spinal deformities. *Medical and Biological Engineering and Computing*, 45(6) :591–602, 2007.
- [2] W. Mollemans, F. Schutyser, N. Nadjmi, F. Maes, and P. Suetens. Predicting soft tissue deformations for maxillofacial surgery planning system : from computational strategies to a complete clinical validation. *Medical Image Analysis*, 11(3) :282–301, 2007.
- [3] C.-E. Aubin, H. Labelle, and O. C. Ciolofan. Variability of spinal instrumentation configurations in adolescent idiopathic scoliosis. *European Spine Journal*, 16(1) :57–64, 2007.
- [4] C.-E. Aubin, H. Labelle, C. Chevretil, G. Desroches, J. Clin, and A. B. Eng. Preoperative planning simulator for spinal deformity surgeries. *Spine*, 33(20) :2143–2152, 2008.
- [5] V. J. Raso, E. Lou, D. L. Hill, J. K. Mahood, M. J. Moreau, and N. G. Durdle. Trunk distorsion in adolescent idiopathic scoliosis. *J.Pediatr. Orthop.*, 18 :222–226, 1998.
- [6] C. Denoel, M. F. I. Aguirre, G. Bianco, P. H. Mahaudens, R. Vanwijck, S. Garson, R. Sinna, and A. Debrun. Idiopathic scoliosis and breast asymmetry. *Journal of Plastic Reconstructive and Aesthetic Surgery*, 62 :1303–1308, 2009.
- [7] T. G. Lowe, M. Edgar, J. Y. Margulies, N. H. Miller, V. J. Raso, K. A. Reinker, and C. H. Rivard. Etiology of idiopathic scoliosis : current trends in research. *J Bone Joint Surg Am*, 82-A :1157–1168, 2000.
- [8] E. J. Rogala, D. S. Drummond, and J. Gurr. Scoliosis : incidence and natural history. a prospective epidemiological study. *J Bone Joint Surg Am*, 60 :173–176, 1978.
- [9] J.R. Cobb. Outline for the study of scoliosis. *Am. Acad. Orthop. Surg. Instruct. Lect.*, 5 :261–275, 1948.
- [10] S. Negrini. Bracing adolescent idiopathic scoliosis today. *Disabil Rehabil Assist Technol*, 3 :107–111, 2008.
- [11] R.R. Betz and H. Shufflebarger. Anterior versus posterior instrumentation for the correction of thoracic idiopathic scoliosis. *Spine*, 26(9) :1095–1100, 2001.

- [12] P. Papin, H. Labelle, S. Delorme, C.E. Aubin, J.A. De Guise, and J. Dansereau. Long-term three-dimensional changes of the spine after posterior spinal instrumentation and fusion in adolescent idiopathic scoliosis. *European Spine Journal*, 8(1) :16–21, 1999.
- [13] S. Delorme, P. Violas, J. Dansereau, J. de Guise, C.-E. Aubin, and H. Labelle. Preoperative and early postoperative three-dimensional changes of the rib cage after posterior instrumentation in adolescent idiopathic scoliosis. *European Spine Journal*, 10(2) :101–107, 2001.
- [14] M. Asher, S. M. Lai, D. Burton, and B. Manna. Maintenance of trunk deformity correction following posterior instrumentation and arthrodesis for idiopathic scoliosis. *Spine*, 29 :1782–1788, 2004.
- [15] R. K. Pratt, J. K. Webb, R. G. Burwell, and A. A. Cole. Changes in surface and radiographic deformity after universal spine system for right thoracic adolescent idiopathic scoliosis : is rib-hump reassertion a mechanical problem of the thoracic cage rather than an effect of relative anterior spinal overgrowth ? *Spine*, 26 :1778–1787, 2001.
- [16] U. Willers, E. E. Transfeldt, and R. Hedlund. The segmental effect of cotrel-dubousset instrumentation on vertebral rotation, rib hump and the thoracic cage in idiopathic scoliosis. *European Spine Journal*, 5(6) :387–393, 1996.
- [17] T. R. Haheer, A. Merola, R. I. Zipnick, J. Gorup, D. Mannor, and J. Orchowski. Meta-analysis of surgical outcome in adolescent idiopathic scoliosis. a 35-year english literature review of 11,000 patients. *Spine*, 20(14) :1575–1584, 1995.
- [18] A. E. Geissele, J. W. Ogilvie, M. Cohen, and D. S. Bradford. Thoracoplasty for the treatment of rib prominence in thoracic scoliosis. *Spine*, 19(14) :1636–1642, 1994.
- [19] K.H. Bridwell. Surgical treatment of idiopathic adolescent scoliosis. *Spine*, 24(24) :2607–2616, 1999.
- [20] C.-E. Aubin, J. Dansereau, F. Parent, H. Labelle, and J. A. de Guise. Morphometric evaluations of personalised 3d reconstructions and geometric models of the human spine. *Medical and Biological Engineering and Computing*, 35(6) :611–618, 1997.
- [21] D. Périé, C. E. Aubin, M. Lacroix, Y. Lafon, and H. Labelle. Biomechanical modelling of orthotic treatment of the scoliotic spine including a detailed representation of the brace-torso interface. *Medical and Biological Engineering and Computing*, 42 :339–344, 2004.

- [22] J. Carrier, C.-E. Aubin, I. Villemure, and H. Labelle. Biomechanical modelling of growth modulation following rib shortening or lengthening in adolescent idiopathic scoliosis. *Medical and Biological Engineering and Computing*, 42(4) :541–548, 2004.
- [23] Clin J., Aubin C.-E., Parent S., Ronsky J., and Labelle H. Biomechanical modeling of brace design. *Stud. Health Technol. Inform.*, 123 :255–260, 2006.
- [24] J. Clin, C.-E. Aubin, and H. Labelle. Virtual prototyping of a brace design for the correction of scoliotic deformities. *Medical and Biological Engineering and Computing*, 45(5) :467–473, 2007.
- [25] J. Clin, C.-E. Aubin, S. Parent, A. Sangole, and H. Labelle. Comparison of the biomechanical 3D efficiency of different brace designs for the treatment of scoliosis using a finite element model. *Eur. Spine J.*, 19(7) :1169–1178, 2010.
- [26] J. Clin, C.-E. Aubin, S. Parent, and H. Labelle. A biomechanical study of the charleston brace for the treatment of scoliosis. *Spine*, Publish Ahead of Print, 2010.
- [27] J. Clin, C.-E. Aubin, H. Labelle, and S. Parent. Immediate correction in brace treatment : how much is needed to obtain a long-term effectiveness ? In *8th Meeting of the International Research Society of Spinal Deformities (IRSSD 2010)*, Montréal, Québec, Canada, 2010.
- [28] M. Beauséjour, C.E. Aubin, A.G. Feldman, and H. Labelle. Simulations de tests d’inflexion latérale à l’aide d’un modèle musculo-squelettique du tronc. *Annales de chirurgie*, 53 :742–750, 1999.
- [29] O. Dionne, K. C. Assi, S. Grenier, H. Labelle, F. Guibault, and F. Cheriet. Simulation of the postoperative trunk appearance in scoliotic surgery. In *International Symposium On Biomedical Imaging, ISBI 2012*, pages 1208–1211, 2012.
- [30] U. Meier, O. López, C. Monserrat, M. C. Juan, and M. Alcaniz. Real-time deformable models for surgery simulation : a survey. *Computer Methods and Programs Biomedicine*, 77(3) :183–197, 2005.
- [31] R. M. Koch, M. H. Gross, F. R. Carls, D. F. von Büren, G. Fankhauser, and Y. I. H. Parish. Simulating facial surgery using finite element models. In *Proceedings of the 23rd annual conference on Computer graphics and interactive techniques*, pages 421–428. ACM, 1996.

- [32] R. M. Koch, S. H. M. Roth, M. H. Gross, A. P. Zimmermann, and H. F. Sailor. A framework for facial surgery simulation. In *Proceedings of the 18th spring conference on Computer graphics*, pages 33–42, 2002.
- [33] D. Terzopoulos and K. Waters. Physically-based facial modeling, analysis, and animation. *Journal of Visualization and Computer Animation*, 1(2) :73–80, 1990.
- [34] E. Keeve, S. Girod, and B. Girod. Craniofacial surgery simulation. In *Visualization in Biomedical Computing*, pages 541–546. Springer : Berlin, 1996.
- [35] W. Mollemans, F. Schutyser, J.V. Cleynenbreugel, and P. Suetens. Tetrahedral mass spring model for fast soft tissue deformation. In *Surgery Simulation and Soft Tissue Modeling IS4TM 2003, LNCS 2673*, pages 145–154. Springer : Berlin, 2003.
- [36] M. Bro-Nielsen. Surgery simulation using fast finite elements. In *VBC '96 : Proceedings of the 4th International Conference on Visualization in Biomedical Computing*, pages 529–534. Springer-Verlag, 1996.
- [37] S. Cotin, H. Delingette, and N. Ayache. Real-time elastic deformations of soft tissues for surgery simulation. *IEEE Transactions On Visualization and Computer Graphics*, 5(1) :62–73, 1999.
- [38] Matthias Müller, Julie Dorsey, Leonard McMillan, Robert Jagnow, and Barbara Cutler. Stable real-time deformations. In *SCA '02 : Proceedings of the 2002 ACM SIGGRAPH/Eurographics symposium on Computer animation*, pages 49–54. ACM, 2002.
- [39] Guillaume Picinbono, Herve Delingette, and Nicholas Ayache. Real-time large displacement elasticity for surgery simulation : Non-linear tensor-mass model. In *MICCAI '00 : Proceedings of the Third International Conference on Medical Image Computing and Computer-Assisted Intervention*, pages 643–652. Springer-Verlag, 2000.
- [40] M. Chabanas, V. Luboz, and Y. Payan. Patient specific finite element model of the face soft tissues for computer-assisted maxillofacial surgery. *Medical Image Analysis*, 7(2) :131–151, 2003.
- [41] Liesbet Roose, Wim De Maerteleire, Wouter Mollemans, and Paul Suetens. Validation of different soft tissue simulation methods for breast augmentation. *International Congress Series*, 1281 :485–490, 2005.
- [42] R. Mahnken and E. Stein. A unified approach for parameter identification of inelastic material models in the frame of the finite element method. *Computer Methods in Applied Mechanics and Engineering*, 136(3-4) :225 – 258, 1996.

- [43] R. Mahnken and E. Stein. Parameter identification for viscoplastic models based on analytical derivatives of a least-squares functional and stability investigations. *International Journal of Plasticity*, 12(4) :451 – 479, 1996.
- [44] R. Mahnken and E. Stein. Parameter identification for finite deformation elastoplasticity in principal directions. *Computer Methods in Applied Mechanics and Engineering*, 147(1-2) :17 – 39, 1997.
- [45] T. Seibert, J. Lehn, S. Schwan, and F.G. Kollmann. Identification of material parameters for inelastic constitutive models : Stochastic simulations for the analysis of deviations. *Continuum Mechanics and Thermodynamics*, 12(2) :95 – 120, 2000.
- [46] T. Harth, S. Schwan, J. Lehn, and F. G. Kollmann. Identification of material parameters for inelastic constitutive models : statistical analysis and design of experiments. *International Journal of Plasticity*, 20(8-9) :1403 – 1440, 2004.
- [47] W. T. D’Arcy. *On Growth and Form*. Cambridge University Press, 1917.
- [48] U. Grenander and M. I. Miller. Computational anatomy : an emerging discipline. *Q. Appl. Math.*, LVI(4) :617–694, 1998.
- [49] Daniel P. Huttenlocher, Gregory A. Klanderman, Gregory A. Kl, and William J. Rucklidge. Comparing images using the hausdorff distance. *IEEE Transactions on Pattern Analysis and Machine Intelligence*, 15 :850–863, 1993.
- [50] Guillaume Charpiat, Olivier Faugeras, and Renaud Keriven. Approximations of shape metrics and application to shape warping and empirical shape statistics. *Found. Comput. Math.*, 5(1) :1–58, 2005.
- [51] *Distance-Based Shape Statistics*, volume 5, 2006.
- [52] D.G. Kendall. Shape manifolds, procrustean metrics, and complex projective spaces. *Bulletin of the London Mathematical Society*, 16(2) :81–121, 1984.
- [53] F. L. Bookstein. Size and shape spaces for landmark data in two dimensions. *Statistical Science*, 1(2) :181–242, 1986.
- [54] Simone Ceolin, William A. P. Smith, and Edwin Hancock. Facial shape spaces from surface normals and geodesic distance. In *DICTA '07 : Proceedings of the 9th Biennial Conference of the Australian Pattern Recognition Society on Digital Image Computing Techniques and Applications*, pages 416–423, Washington, DC, USA, 2007. IEEE Computer Society.

- [55] Simone Ceolin, William Smith, and Edwin Hancock. Facial shape spaces from surface normals. In *Image Analysis and Recognition*, pages 955–965. 2008.
- [56] C. R. Rao. Information and accuracy attainable in estimation of statistical parameters. *Bulletin of the Calcutta Mathematical Society*, 37 :81–91, 1945.
- [57] *Shape analysis using the Fisher-Rao Riemannian metric : unifying shape representation and deformation*, 2006.
- [58] Adrian M. Peter and Anand Rangarajan. Information geometry for landmark shape analysis : Unifying shape representation and deformation. *IEEE Transactions on Pattern Analysis and Machine Intelligence*, 31 :337–350, 2009.
- [59] Simone Ceolin and Edwin R. Hancock. Using the fisher-rao metric to compute facial similarity. In *ICIAR (1)*, pages 384–393, 2010.
- [60] J. Glaunes, A. Trouvé, and L. Younes. Diffeomorphic matching of distributions : A new approach for unlabelled point-sets and sub-manifolds matching. In *In CVPR*, pages 712–718, 2004.
- [61] M. Vaillant and J. Glaunès. Surface matching via currents. In *Proceedings of Information Processing in Medical Imaging (IPMI 2005), number 3565 in Lecture Notes in Computer Science*, pages 381–392, 2005.
- [62] J. Glaunès, A. Qiu, M. I. Miller, and L. Younes. Large deformation diffeomorphic metric curve mapping. *Int. J. Comput. Vision*, 80(3) :317–336, 2008.
- [63] S. Durrleman, X. Pennec, A. Trouvé, and N. Ayache. Statistical models of sets of curves and surfaces based on currents. *Medical Image Analysis*, 13(5) :793–808, 2009. Includes Special Section on the 12th International Conference on Medical Imaging and Computer Assisted Intervention.
- [64] N. Acir and C. Guzelis. Automatic spike detection in eeg by a two-stage procedure based on support vector machines. *Computers in Biology and Medicine*, 34(7) :561–575, 2004.
- [65] G.-Z. Li, J. Yang, C.-Z. Ye, and D.-Y. Geng. Degree prediction of malignancy in brain glioma using support vector machines. *Comput. Biol. Med.*, 36(3) :313–325, 2006.
- [66] C. Bergeron, F. Cheriet, J. Ronsky, R. Zernicke, and H. Labelle. Prediction of anterior scoliotic spinal curve from trunk surface using support vector regression. *Eng. Appl. Artificial Intell.*, 18(8) :973–983, 2005.

- [67] J. Jaremko, P. Poncet, J. Ronsky, J. Harder, J. Harder, J. Dansereau, H. Labelle, and R. Zernicke. Genetic algorithm-neural network estimation of cobb angle from torso asymmetry in scoliosis. *J. Biomech. Eng.*, 124(5) :496–503, 2002.
- [68] L. Ramirez, N.G. Durdle, V.J. Raso, and D.L. Hill. A support vector machines classifier to assess the severity of idiopathic scoliosis from surface topography. *IEEE Trans. Inf. Technol. Biomed.*, 10(1) :84–91, 2006.
- [69] L. Seoud, M.M. Adankon, H. Labelle, J. Dansereau, and F. Cheriet. Prediction of scoliosis curve type based on the analysis of trunk surface topography. In *Biomedical Imaging : From Nano to Macro, 2010 IEEE International Symposium on*, pages 408–411, 2010.
- [70] T.M. Cover and P.E. Hart. Nearest neighbor pattern classification. *IEEE Transactions on Information Theory*, IT-13 :21–27, 1967.
- [71] T. M. Cover. Estimation by the nearest neighbor rule. *IEEE Transactions on Information Theory*, IT-14(1) :50–55, 1968.
- [72] L. Devroye, L. Györfi, A. Krzyżak, and G. Lugosi. On the strong universal consistency of nearest neighbor regression function estimates. *The Annals of Statistics*, 22 :1371–1385, 1994.
- [73] S. R. Kulkarni and S. E. Posner. Rates of convergence of nearest neighbor estimation under arbitrary sampling. *IEEE Trans. Inf. Theory*, 41 :1028–1039, 1995.
- [74] G. Biau, F. Cérou, and A. Guyader. Rates of convergence of the functional k-nearest neighbor estimate. *IEEE Transactions on Information Theory*, 56 :2034–2040, 2010.
- [75] Kilian Weinberger, John Blitzer, and Lawrence Saul. Distance metric learning for large margin nearest neighbor classification. In Y. Weiss, B. Schölkopf, and J. Platt, editors, *Advances in Neural Information Processing Systems 18*, pages 1473–1480. MIT Press, Cambridge, MA, 2006.
- [76] K. Weinberger and L. Saul. Fast solvers and efficient implementations for distance metric learning. pages 1160–1167, 2008.
- [77] K.Q. Weinberger and L.K. Saul. Distance metric learning for large margin nearest neighbor classification. *Journal of Machine Learning Research*, 10.
- [78] C. Domeniconi, J. Peng, and D. Gunopulos. Locally adaptive metric nearest neighbor classification. *IEEE Trans. Pattern Anal. Mach. Intell.*, 24(9) :1281–1285, 2002.

- [79] T. Hastie and R. Tibshirani. Discriminant adaptive nearest neighbor classification. *IEEE Trans. Pattern Anal. Mach. Intell.*, 18(6) :607–615, 1996.
- [80] Y. Lee, D. Terzopoulos, and K. Waters. Realistic modeling for facial animation. In *SIGGRAPH '95 : Proceedings of the 22nd annual conference on Computer graphics and interactive techniques*, pages 55–62, New York, NY, USA, 1995. ACM.
- [81] S. Sarni, A. Maciel, R. Boulic, and D. Thalmann. Evaluation and visualization of stress and strain on soft biological tissues in contact. In *SMI '04 : Proceedings of the Shape Modeling International 2004*, pages 255–262, Washington, DC, USA, 2004. IEEE Computer Society.
- [82] S. Delorme, Y. Petit, J. A. de Guise, H. Labelle, C.-E. Aubin, and J. Dansereau. Assessment of the 3D reconstruction and high-resolution geometrical modeling of the human skeletal trunk from 2D radiographic images. *IEEE Transactions on Biomedical Engineering*, 50(8) :989–98, 2003.
- [83] H. Si. Tetgen : A quality tetrahedral mesh generator and three-dimensional delaunay triangulator. <http://tetgen.berlios.de/>.
- [84] J. R. Shewchuk. Tetrahedral mesh generation by delaunay refinement. In *SCG '98 : Proceedings of the fourteenth annual symposium on Computational geometry*, pages 86–95. ACM, 1998.
- [85] M. Teschner, B. Heidelberger, M. Müller, and M. Gross. A versatile and robust model for geometrically complex deformable solids. In *Proceedings of the Computer Graphics International*, pages 312–319. IEEE Computer Society, 2004.
- [86] J. L. Jaremko, P. Poncet, J. Ronsky, J. Harder, and J. Dansereau. Indices of torso asymmetry related to spinal deformity in scoliosis. *Clinical Biomechanics*, 17(8) :559–568, 2002.
- [87] L. Seoud, F. Cheriet, H. Labelle, and J. Dansereau. A novel method for the 3d reconstruction of scoliotic ribs from frontal and lateral radiographs. *IEEE Transactions in biomedical engineering*, 58(5) :1135–1146, 2011.
- [88] V. Pazos, F. Cheriet, J. Dansereau, Janet Ronsky, Ronald F. Zernicke, and Hubert Labelle. Reliability of trunk shape measurements based on 3-d surface reconstructions. *European Spine Journal*, 16(11) :1882–1891, 2007.

- [89] R. Buchanan, J. G. Birch, A. A. Morton, and R. H. Browne. Do you see what I see? Looking at scoliosis surgical outcomes through orthopedists' eyes. *Spine*, 28(24) :2700–2704, 2003.
- [90] Goran Devedzic, Sasa Cukovic, Vanja Lukovic, Danijela Milosevic, K. Subburaj, and Tanja Lukovic. Scoliomedis : Web-oriented information system for idiopathic scoliosis visualization and monitoring. *Computer Methods and Programs in Biomedicine*, 108(2) :736–749, 2012.
- [91] V. Pazos, F. Cheriet, H. Labelle, and J. Dansereau. 3d reconstruction and analysis of the whole trunk surface for non-invasive follow-up of scoliotic deformities. *Studies in health technology and informatics*, 91 :296–299, 2002.
- [92] T.M.L. Shannon. *Dynamic Surface Topography and Its Application to the Evaluation of Adolescent Idiopathic Scoliosis*. PhD thesis, Oxford Brookes University, Oxford, U.K., september 2010.
- [93] Peter O. Ajemba, Nelson G. Durdle, and V. James Raso. Characterizing torso shape deformity in scoliosis using structured splines models. *IEEE Trans. Biomed. Engineering*, 56(6) :1652–1662, 2009.
- [94] S. Li, W. Zhou, Q. Yuan, S. Geng, and D. Cai. Feature extraction and recognition of ictal eeg using emd and svm. *Computers in Biology and Medicine*, 43(7) :807–816, 2013.
- [95] A. Subasi. Classification of emg signals using pso optimized svm for diagnosis of neuromuscular disorders. *Computers in Biology and Medicine*, 43(5) :576–586, 2013.
- [96] E. Comak, A. Arslan, and I. Türkoglu. A decision support system based on support vector machines for diagnosis of the heart valve diseases. *Computers in biology and Medicine*, 37(1) :21–27, 2007.
- [97] S. Kiranyaz, T. Ince, J. Pulkkinen, M. Gabbouj, J. Ärje, S. Kärkkäinen, V. Tirronen, M. Juhola, T. Turpeinen, and K. Meissner. Classification and retrieval on macroinvertebrate image databases. *Computers in Biology and Medicine*, 41(7) :463–472, 2011.
- [98] H. M. Muda, P. Saad, and R. M. Othman. Remote protein homology detection and fold recognition using two-layer support vector machine classifiers. *Computers in Biology and Medicine*, 41(8) :687–699, 2011.
- [99] T. Hastie, R. Tibshirani, and Friedman. *The elements of statistical learning*.

- [100] H. Hotelling. Analysis of a complex of statistical variables into principal components. *Journal of Educational Psychology*, 24 :417—441, 1933.
- [101] B. Schölkopf, A.J. Smola, and K.-R. Müller. Nonlinear component analysis as a kernel eigenvalue problem. *Neural Computation*, 10(5) :1299–1319, 1998.
- [102] X. He and P. Niyogi. *Locality Preserving Projections*. Cambridge, MA, 2004. MIT Press.
- [103] X. He, D. Cai, S. Yan, and H.-J. Zhang. Neighborhood preserving embedding. In *Proceedings of IEEE International Conference on Computer Vision*, volume 2, pages 1208–1213. IEEE, 2005.
- [104] H. Wold. Soft Modeling by Latent Variables; the Nonlinear Iterative Partial Least Squares Approach. *Perspectives in Probability and Statistics. Papers in Honour of M. S. Bartlett*, 1975.
- [105] S. Wold, H. Ruhe, H. Wold, and W.J. Dunn III. The collinearity problem in linear regression. the partial least squares (PLS) approach to generalized inverse. *SIAM Journal of Scientific and Statistical Computations*, 5(3) :735–743, 1984.
- [106] V. Pazos, F. Cheriet, L. Song, H. Labelle, and J. Dansereau. Accuracy assessment of human trunk surface 3d reconstructions from an optical digitizing system. *Medical and Biological Engineering and Computing*, 43(1) :11–15, 2005.
- [107] J.A.K. Suykens, V.T. Gestel, J. De Brabanter, B. De Moor, and J. Vandewalle. *Least Squares Support Vector Machines*. World Scientific, Singapore, 2002.
- [108] S.-M. Huang and J.-F. Yang. Unitary regression classification with total minimum projection error for face recognition. *IEEE signal processing letters*, 20(5) :443–446, 2013.
- [109] B.L. Pellom, R. Sarikaya, and J.H.L. Hansen. Fast likelihood computation techniques in nearest-neighbor based search for continuous speech recognition. *IEEE Signal Processing Letters*, 8(8) :221–224, 2001.
- [110] S. Marano, V. Matta, and P. Willett. Nearest-neighbor distributed learning by ordered transmissions. *IEEE Transactions on Signal Processing*, 61(21) :221–224, 2013.
- [111] Dor Kedem, Stephen Tyree, Kilian Weinberger, Fei Sha, and Gert Lanckriet. Non-linear metric learning. In P. Bartlett, F.C.N. Pereira, C.J.C. Burges, L. Bottou, and K.Q.

- Weinberger, editors, *Advances in Neural Information Processing Systems 25*, pages 2582–2590. 2012.
- [112] B. Kulis. Metric learning : A survey. *Foundations and Trends in Machine Learning*, 5(4) :287–364, 2013.
- [113] J. Devore and N. Farnum. *Applied Statistics for Engineers and Scientists*. Duxbury Press, 1999.
- [114] C.-É. Aubin, Y. Petit, I.A.F. Stokes, F. Poulin, M. Gardner-Morse, and H. Labelle. Biomechanical modeling of posterior instrumentation of the scoliotic spine. *Computer Methods in Biomechanics and Biomedical Engineering*, 6(1) :27–32, 2003.
- [115] S. Cotin, H. Delingette, and N. Ayache. A hybrid elastic model allowing real-time cutting, deformations and force-feedback for surgery training and simulation. *The Visual Computer*, 16 :437–452, 2000.
- [116] R. Harmouche, F. Cheriet, H. Labelle, and J. Dansereau. 3D registration of MR and X-ray spine images using an articulated model. *Computerized Medical Imaging and Graphics*, 36(5) :410 – 418, 2012.
- [117] K.M Cheung and K.D Luk. Prediction of correction of scoliosis with se of the fulcrum bending radiograph. *J. Bone Joint Surg. Am.*, 79 :1144–1150, 1997.
- [118] P. Debanné, V. Pazos, H. Labelle, and F. Cheriet. Evaluation of reducibility of trunk asymmetry in lateral bending. In *8th Meeting of the International Research Society of Spinal Deformities (IRSSD 2010)*, Montréal, Québec, Canada, 2010.